

Counter-rotating standing spin waves: A magneto-optical illusion

S. Shihab, L. Thevenard, A. Lemaître, C. Gourdon

▶ **To cite this version:**

S. Shihab, L. Thevenard, A. Lemaître, C. Gourdon. Counter-rotating standing spin waves: A magneto-optical illusion. Physical Review B, 2017, 95 (14), pp.144411. 10.1103/PhysRevB.95.144411 . hal-01490261

HAL Id: hal-01490261
https://hal.science/hal-01490261

Submitted on 15 Mar 2017

HAL is a multi-disciplinary open access archive for the deposit and dissemination of scientific research documents, whether they are published or not. The documents may come from teaching and research institutions in France or abroad, or from public or private research centers.

L'archive ouverte pluridisciplinaire **HAL**, est destinée au dépôt et à la diffusion de documents scientifiques de niveau recherche, publiés ou non, émanant des établissements d'enseignement et de recherche français ou étrangers, des laboratoires publics ou privés.

Counter-rotating standing spin-waves: a magneto-optical illusion

S. Shihab,[1] L. Thevenard,[1] A. Lemaître,[2] and C. Gourdon[1,*]

[1] *Sorbonne Universités, UPMC Univ Paris 06, CNRS-UMR 7588, Institut des NanoSciences de Paris, F-75005, Paris, France*

[2] *Centre de Nanosciences et Nanotechnologies, CNRS, Univ. Paris-Sud, Université Paris-Saclay, 91460 Marcoussis, F-91460 France*

(Dated: January 13, 2017)

We excite perpendicular standing spin waves by a laser pulse in a GaMnAsP ferromagnetic layer and detect them using time-resolved magneto-optical effects. Quite counter-intuitively, we find the first two excited modes to be of opposite chirality. We show that this can only be explained by taking into account absorption and optical phase shift inside the layer. This optical illusion is particularly strong in weakly absorbing layers. These results provide a correct identification of spin waves modes, enabling a trustworthy estimation of their respective weight as well as an unambiguous determination of the spin stiffness parameter.

PACS numbers: 75.78.Jp ,75.30.Ds,75.50.Pp

Since pioneering work on nickel [1], laser-induced magnetization dynamics has been widely used to investigate ultrafast magnetic processes not only in magnetic metals [2, 3], but also in magnetic semiconductors [4–9] and insulators [10, 11], exploring the fundamentals of light-spin interaction in view of a full and ultrafast optical control of magnetic order.

Ultrashort pulses can trigger a wide variety of processes, including ultrafast demagnetization [1], full magnetization reversal [12] as well as coherent precession [2, 4, 10]. In magnetically ordered materials, ferro- and ferrimagnets, as well as in antiferromagnets, the coherent magnetization dynamics arises from collective spin excitations, spin waves (SW) (or magnons, their quanta), which attract a considerable interest motivated by their possible use as information carriers in magnonics applications [13, 14]. Magnons are versatile excitations since their dispersion curves, comprising magnetostatic and exchange modes [15], can be tuned by a magnetic field or by micro- or nanostructuring the material in any of its dimensions [14]. For instance, perpendicular standing spin-wave (PSSW) modes in a single nanometric layer of thickness L with free boundary conditions (no surface anisotropy) will have their wave-vector quantized by an integer p ($k = p\pi/L$), and their energy by p^2, proportionally to the spin stiffness D.

SWs can be studied in the frequency domain by, *e.g.*, ferromagnetic resonance (FMR) experiments or Brillouin light scattering as well as in the time-domain by time-resolved laser pump-probe (PP) experiments using magneto-optical effects. The latter distinguish themselves in various ways from the former. The *coherent* excitation of several PSSWs with different frequencies, from the sub-GHz to the THz range, is made possible by the wide frequency spectrum of the pulsed excitation induced by the femtosecond pump laser pulses. In a single time-scan PP experiments can detect several coherent SW modes, and provide their time period, their respective phases and their damping. Coherent control experiments using two pump beams can be performed [16, 17]. Furthermore the possibility to fully reconstruct the magnetization trajectory using two different magneto-optical effects [18, 19] brings a deep insight into magnetization dynamics.

Whereas the excitation mechanism of SWs by optical, acoustical or magnetic field pulses [14, 20–22], has been thoroughly discussed, their optical detection has been much less addressed [4, 23]. In particular, in contrast to the cavity FMR detection of SWs which was modeled a long time ago [24], the respective amplitudes of optically detected SWs remained unexplained [2, 9, 14, 25]. In this Letter, we provide a comprehensive model to explain the large amplitude of these non-uniform SWs that should not be detectable in the framework of simple models [4]. We moreover present intriguing experimental results of apparent different chiralities for SWs of different parities. We show that they can only be explained by this theoretical description of the magneto-optical detection through the Kerr and Voigt effects that takes into account the absorption depth and the optical phase shift inside the layer. Important consequences are expected when the SW wavelength (determined by the layer thickness) becomes a few tenth of the wavelength of light in the material, λ/η, where η is the refractive index. In particular, ignoring this effect can lead to an erroneous determination of the SW stiffness, and of the relative mode amplitude, a signature of the up-to-now elusive magnon excitation mechanisms. We show that the optical phase shift can lead to a striking and non-intuitive optical effect in the detection of SWs: an apparent reversal of the magnetization rotation direction for SWs of odd parity with respect to the layer mid-plane. A key result of this paper is that the optical phase shift provides a unique tool for the determination of the SW mode number, or in other words its parity.

We study thin layers of the ferromagnetic semiconduc-

tor alloy GaMnAsP. Most samples show only one PSSW mode in the FMR spectra while one or two modes are optically detected in the TRMO signal [8, 29]. The results presented here are obtained in an in-plane magnetized GaMnAsP layer with thickness L=50 nm and Phosphorus concentration 4.3 % grown on a (001) GaAs substrate by molecular beam epitaxy and annealed 1 hour at 250°C. The effective Mn concentration is 4 % and the Curie temperature is 85 K. The anisotropy constants were determined by FMR. PP experiments are carried out at T=12 K in zero external magnetic field after a 60 mT in-plane initialization of the magnetization direction. The laser source is a 76 MHz Ti:Sapphire laser at a wavelength λ=700 nm. To limit thermal effects, low pump and probe fluence are used (1 μJ cm^{-2} and 0.4 μJ cm^{-2}, respectively) [30]. The pump beam is modulated at 50 kHz. The pump-induced magnetization dynamics is detected as a function of the pump-probe delay through the rotation of the probe beam linear polarization detected by a balanced optical diode bridge and a lock-in amplifier. The static rotation and ellipticity signals are obtained with the probe beam only.

The existence of circular and linear magnetic birefringence/dichroism [31] makes the TRMO signal sensitive to both the out-of-plane $\delta\theta$ and the in-plane $\delta\phi$ components of the transient magnetization (Fig. 1(a)). This allows for the reconstruction of the magnetization trajectory using the expected dependency of the rotation angle $\delta\beta_r$ on the probe polarization angle β (Ref. 19 and Suppl-info):

$$\delta\beta_r^{exp}(t) = K_r\delta\theta_{exp}(t) + 2V_r\delta\phi_{exp}(t)\cos 2(\beta-\phi_0) - 2V_r\frac{\delta M(t)}{M}\sin 2(\beta-\phi_0)\ , \quad (1)$$

where K_r and V_r are the static Kerr and Voigt rotation coefficients, M is the magnetization vector modulus, and ϕ_0 is the in-plane equilibrium angle of the magnetization. Figure 1(b) shows the dependence of the TRMO signal on the incident probe polarization. The signal is fitted with $u(t)+v(t)\sin 2\beta + w(t)\cos 2\beta$ from which we obtain the $\delta\theta_{exp}(t)$ and $\delta\phi_{exp}(t)$ functions taking into account the magnetization equilibrium angle ϕ_0 ($\boldsymbol{M}$ close to [100]) as shown in Fig. 1(c) (see Suppl-info). The plot of the trajectory, $\delta\theta_{exp}(t)$ versus $\delta\phi_{exp}(t)$ shown in Fig. 1(d) reveals a very complex dynamics that actually results from the contributions of two SWs that clearly appear in $\delta\theta_{exp}(t)$ and $\delta\phi_{exp}(t)$ and their Fourier transform (Fig. 1(c) and inset). Let us note the large ratio ($\approx$ 0.6) of the amplitude of the second SW with respect to the first one. $\delta\theta_{exp}(t)$ and $\delta\phi_{exp}(t)$ are fitted with two damped oscillating signals and a sum of two exponentials that reflects the shape of the laser-induced pulsed excitation (τ_1=0.03 ns, τ_2=1 ns). Plotting separately the trajectory for each SW (f_0=2.36 GHz and f_1=3.90 GHz) in Fig. 1(e, f) results in a much clearer picture of the magnetization precession. Surprisingly, the magnetization seems to rotate in *opposite* directions for the two SWs. As we shall see below, this is an "optical illusion" resulting from an optical phase shift inside the layer. To demonstrate this, we first describe the SW excitation by a laser pulse using the Landau-Lifshitz-Gilbert (LLG) equation and appropriate boundary conditions at the top and bottom interfaces. We then calculate the detected magneto-optical signal using a multi-layer and transfer matrix model, which we show to be indispensable to recover the observed SWs chiralities.

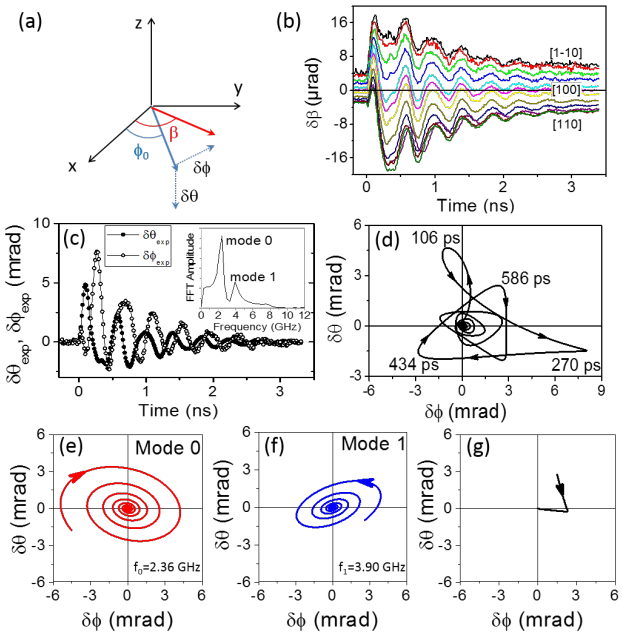


FIG. 1. (a) Reference frame. (b) Dependence of the TRMO signal $\delta\beta$ on the probe beam linear polarization with respect to the sample crystallographic axes. (c) Time dependence of $\delta\theta_{exp}$ and $\delta\phi_{exp}$. Inset: Fourier transform amplitude of $\delta\theta_{exp}$. (d) Optically detected magnetization trajectory. (e), (f), (g) Decomposition of the experimental magnetization trajectory (d) into two oscillating signals at frequencies f_0=2.36 GHz and f_1=3.90 GHz and a non-oscillating signal, respectively.

The SW space and time profiles are obtained by solving the LLG equation within the small precession angle approximation for in-plane static magnetization:

$$\dot{\delta\phi} = \gamma\Big(F_{\theta\theta}\ \delta\theta - D\frac{\partial^2\delta\theta}{\partial z^2}\Big) + \alpha_G\dot{\delta\theta}$$
$$\dot{\delta\theta} = -\gamma\Big(F_{\phi\phi}\ \delta\phi - D\frac{\partial^2\delta\phi}{\partial z^2} + \delta B_{exc}(z,t)\Big) - \alpha_G\ \dot{\delta\phi}\ . \quad (2)$$

F is equal to E/M where E is the magnetic anisotropy energy [28]. α_G is the Gilbert damping. $F_{i,j} = \frac{\partial^2 F}{\partial i\partial j}$ are the second derivatives of F with respect to the angles (i,j). Since it was shown that in thin (Ga,Mn)(As,P) layers the lowest frequency PSSW is a nearly uniform mode, independent of the layer thickness [8, 9], the boundary conditions at z=0 and $z=L$ were chosen to ensure very weak surface pinning, giving nearly flat $\delta\theta(z)$ and $\delta\phi(z)$

profiles at any t for this mode (see Suppl-info). Under symmetric conditions the p-PSSW eigenmodes (p=0, 1, 2...) are even (odd) with respect to the layer mid-plane for even (odd) p. $\delta B_{exc}(z,t)$ is the optically induced effective field that launches the magnetization precession. It arises from the in-plane rotation of the magnetic easy axis induced by transient thermal effects or by the optical spin-orbit torque [32]. $\delta B_{exc}(z,t)$ is taken as a product of time and space functions $f(t)g(z)$. $f(t)$ is chosen so that the calculated $\delta\theta(t)$ and $\delta\phi(t)$ match the experimental ones. $g(z)$ is taken as a Fourier series over the PSSW eigenmodes (see Suppl-info). The depth dependence of the magnetization trajectory for the p=0, 1, 2 SW modes (with time dependence $\cos(2\pi f_p t+\phi_p)$) is shown in Fig. 2 (a-c), respectively. It is seen that inside the layer the direction of rotation is the same for the three modes. For modes 1 and 2 the magnetization vector experiences a π-shift at each node, but its direction of rotation does not change with z (Fig. 2(b,c)).

The TRMO signal is then calculated using a multilayer and transfer matrix model to obtain the Kerr and Voigt rotation angle and ellipticity. The magnetic layer of thickness L is divided in N sub-layers with magnetization components $M(m_{x,y}+\delta m_{x,y,z}(z_i,t))$ (Fig. S1 of Suppl-info). The calculation is performed for normal incidence of light along the z-direction and linear polarization making an angle β with the x-axis. The theoretical dynamical polarization rotation $\delta\beta_r^{th}(t)$ is obtained by taking the limit of an infinite number of sub-layers ($N\to\infty$). $\delta\beta_r^{th}(t)$ is the sum of the Kerr and Voigt rotation angles, $\delta\beta_r^{th}(t)=\delta\beta_{K_r}^{th}(t)+\delta\beta_{V_r}^{th}(t)\cos 2(\beta-\phi_0)$ with:

$$\delta\beta_{K_r}^{th}(t)=-\frac{4\pi}{\lambda}\mathrm{Re}\left[\frac{n^2Q}{n^2-1}\int_0^L e^{i\frac{4\pi nz}{\lambda}}\delta\theta(z,t)dz\right]$$
$$\delta\beta_{V_r}^{th}(t)=\frac{4\pi}{\lambda}\mathrm{Im}\left[\frac{n^2B}{(n^2-1)}\int_0^L e^{i\frac{4\pi nz}{\lambda}}\delta\phi(z,t)dz\right]\ , \quad (3)$$

where $B=B_1+Q^2$. Q ($\propto M$) and B_1 ($\propto M^2$) are the elements of the dielectric permittivity tensor describing the Kerr and Voigt effects, respectively (see Suppl-info). $n=\eta+i\kappa$ is the layer mean complex refractive index and $e^{i\frac{4\pi nz}{\lambda}}=e^{-\alpha z}e^{i\frac{4\pi\eta z}{\lambda}}$ with $\alpha=\frac{4\pi\kappa}{\lambda}$ the absorption coefficient.

The important result is the modulation of the spatial dependence of the $\delta\theta(z,t)$ and $\delta\phi(z,t)$ magnetization components by the optical phase factor $e^{i\frac{4\pi\eta z}{\lambda}}$ that reflects the propagation of light from the surface to the depth z and back. The phase factor is damped by the $e^{-\alpha z}$ absorption factor. Therefore, in the case of strong absorption as in metallic layers, the TRMO signal will be sensitive only to the SW amplitude very close the surface within the absorption depth. In the case of weak absorption and layer thickness L comparable to a fraction of the light wavelength inside the material λ/η, the optical phase shift plays a crucial role. It is precisely the case of the sample studied here where $L\approx\lambda/4\eta$.

Actually, for static magnetization, the importance of a phase shift factor that makes the magneto-optical effects sensitive to the magnetization at a specific depth inside single or multiple ferromagnetic layers was theoretically pointed out [33, 34] and evidenced experimentally in the 90s [35] and recently in GaMnAs layers [36]. Similar ideas were at play when conceiving magneto-optical sensors using magnetic quantum wells in optical cavities [37] or magneto-photonic crystals with enhanced Faraday rotation [38, 39]. However, these ideas had so far not been applied to the time-resolved optical detection of PSSWs in ferromagnetic layers.

The dynamical rotation angles $\delta\beta_{K_r}^{th}(t)$ and $\delta\beta_{V_r}^{th}(t)$ are calculated according to Eq. 3 with the real and imaginary parts of Q and B extracted from the static rotation and ellipticity using Eqs. S12 and S13 of Suppl-info. In order to compare the optically detected magnetization trajectory and the theoretical one we define $\delta\theta_{opt}(z,t)$ and $\delta\phi_{opt}(z,t)$ so that $\delta\beta_r^{th}(t)=K_r\left\langle\delta\theta_{opt}\right\rangle_z(t)+2V_r\left\langle\delta\phi_{opt}\right\rangle_z(t)\cos 2(\beta-\phi_0)$ where $\left\langle\cdots\right\rangle_z=(1/L)\int_0^L\cdots(z)dz$ denotes the average value over the layer thickness, K_r and V_r are given by Eqs. S11 and S18 of Suppl-info, respectively and

$$\delta\theta_{opt}(z,t)=-\frac{1}{K_r}\mathrm{Re}\left[\frac{\phi_{opt}nQ}{(n^2-1)}e^{i\frac{4\pi nz}{\lambda}}\right]\delta\theta(z,t)\ , \quad (4)$$
$$\delta\phi_{opt}(z,t)=\frac{1}{2V_r}\mathrm{Im}\left[\frac{\phi_{opt}nB}{(n^2-1)}e^{i\frac{4\pi nz}{\lambda}}\right]\delta\phi(z,t)\ , \quad (5)$$

with $\phi_{opt}=4\pi nL/\lambda$ the complex optical phase. Figures 2(d-f) show the depth dependence of the $(\delta\phi_{opt},\delta\theta_{opt})$ parametric plot. The effect of the phase factor $e^{i\frac{4\pi nz}{\lambda}}$ is clearly observed when compared to the $(\delta\phi,\delta\theta)$ trajectory shown in Figs 2 (a-c). Despite the difference between Figs 2 (a) and (d), for a uniform SW mode the optically detected trajectory is the same as the simple average of the magnetization dynamics over the layer as expected from the expression of (K_r, Vr) (Eqs. S11, S18) and the definition of ($\delta\theta_{opt}$, $\delta\phi_{opt}$). This is indeed verified on Figs 2 (g,j). The quasi-uniform mode 0 is detected as rotating clockwise (CW) with time as dictated by the sign of the gyromagnetic factor. An opposite rotation direction can be expected for a non-uniform SW mode if the sign of either $\langle\delta\theta_{opt}\rangle$ or $\langle\delta\phi_{opt}\rangle$ is changed with respect to that of $\langle\delta\theta\rangle$ or $\langle\delta\phi\rangle$. This is indeed what is found for the p=1 odd mode, which rotates counter-clock-wise (CCW) as shown in Fig. 2(k). The p=2 mode rotates CW like the $p=0$ mode (Fig. 2(l)).

In order to explain why odd modes may exhibit an apparently inverted direction of rotation when detected optically, we take a simplified model and calculate the sign of the amplitude ratio $\delta\theta_{opt}(t)/\delta\phi_{opt}(t)$. The damped p-PSSW mode at frequency f_p is expressed as $\delta\theta_p(z,t)=a_p^\theta\exp(-\chi_p t)\cos(2\pi f_p t)\cos(p\pi z/L)$, $\delta\phi_p(z,t)=a_p^\phi\exp(-\chi_p t)\sin(2\pi f_p t)\cos(p\pi z/L)$. Ne-

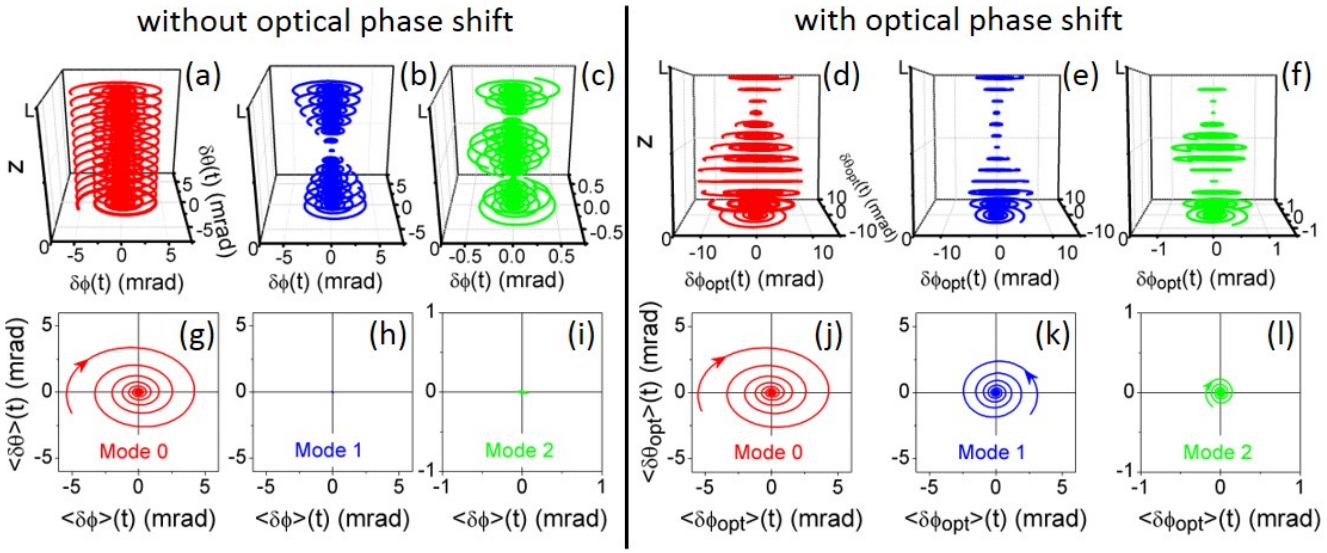


FIG. 2. (left) Magnetization trajectory in the depth of the ferromagnetic layer for the p=0 (a), p=1 (b), p=2 (c) PSSW modes and corresponding detected trajectory in (g), (h), (i) assuming that the optical signal would result from a depth-averaged amplitude. (right) (d), (e), (f) Theoretical effective magnetization trajectory in the depth of the ferromagnetic layer taking into account the optical phase factor and corresponding optically detected trajectory in (j), (k), (l). L=50nm, λ=700 nm, the other parameters are given in Suppl-info.

glecting absorption, the optical precession amplitudes normalized to the excitation amplitudes a_p^θ and a_p^ϕ are:

$$\delta\theta_p^{opt} = -\frac{4\pi}{K_r}\frac{\eta}{\eta^2-1}\int_0^\ell \mathrm{Re}\left[Q\, e^{i4\pi u}\right]\cos\left(p\pi u/\ell\right)du$$

$$\delta\phi_p^{opt} = \frac{4\pi}{2V_r}\frac{\eta}{\eta^2-1}\int_0^\ell \mathrm{Im}\left[B\, e^{i4\pi u}\right]\cos\left(p\pi u/\ell\right)du\ , \quad (6)$$

where $\ell = L/(\lambda/\eta)$. It is straightforward to show that for even p (even modes) the ratio $r_p = \delta\theta_p^{opt}/\delta\phi_p^{opt}$ is positive and equal to 1. For odd modes, r_p can on the contrary be positive or negative depending on the layer thickness and the ratios B_i/B_r and Q_i/Q_r of the imaginary and real parts of B and Q, respectively. It is moreover independent of p and is given by $r_p^{\mathrm{odd}} = -(\frac{B_i}{B_r}C_l + S_l)(\frac{Q_i}{Q_r}C_l + S_l)(C_l - \frac{B_i}{B_r}S_l)^{-1}(C_l - \frac{Q_i}{Q_r}S_l)^{-1}$ with $C_l = \cos(2\pi\ell)$ and $S_l = \sin(2\pi\ell)$. Therefore the possibility to change the sign of only one of the $\delta\theta$ and $\delta\phi$ components (r_p <0) and hence to observe a change of the direction of rotation is achieved exclusively for the *odd* SW modes. This result is not fully conserved when taking into account absorption as can be seen in Fig. 3 where the direction of rotation (CW, CCW) given from the sign of r_p is plotted in (dark/light) gray scale. However, given our parameters, r_1 is always negative for L in the range 26-72 nm encompassing the layer thickness of our sample (50 nm) while r_0 and r_2 are positive. This is an important result of this paper as it provides a tool to identify PSSW modes.

This model also accounts very well for the large amplitude ratio of the high/low frequency modes observed

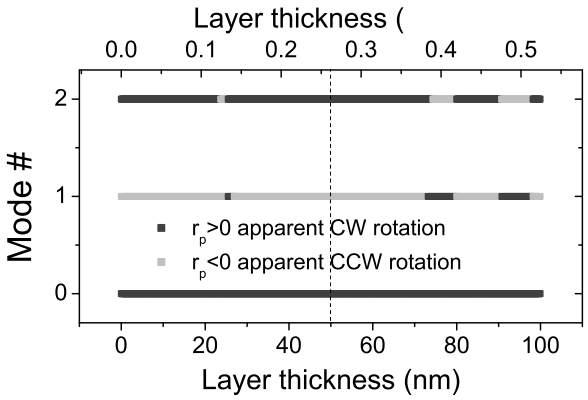


FIG. 3. Theoretical optically detected direction of rotation of the magnetization vector for p=0, 1, and 2 PSSWs modes from the amplitude ratio r_p of $\delta\theta_p^{opt}$ and $\delta\phi_p^{opt}$ (see text). The dashed line indicates the layer thickness. λ=700 nm, η=3.67, κ=0.1.

experimentally. If the optically detected signal were proportional to the average of $\delta\theta$ or $\delta\phi$ over the layer thickness [4], $\langle\delta\theta\rangle_z$ and $\langle\delta\phi\rangle_z$, only the uniform PSSW mode should be detected in the case of free boundary conditions, all the higher ones having zero integral. This is illustrated in Fig. 2(h,i) where the calculated $(\langle\delta\theta\rangle, \langle\delta\theta\rangle)$ signal is zero for the odd p=1 mode and very small for the $p = 2$ mode (it would be strictly zero for zero surface anisotropy). In order to observe higher modes a strong surface pinning would be necessary to give them a non-

zero integral. Even then, only the even modes would be detectable since the odd ones would keep a zero integral for symmetric boundary conditions [4] . Our results definitely prove that the high-frequency mode is the first odd mode. This reconciles results obtained by different groups on the determination of the spin stiffness constant that differ by a factor of 4 depending on whether the high-frequency PSSW mode is identified as the $p = 1$ or $p = 2$ mode [8, 29]. Furthermore it explains why the TRMO signal can show PSSW modes that are not observed in FMR spectra.

In this Letter we have highlighted the role of the optical phase shift in the amplitude of optically detected SW modes. This solves the mystery of counter-rotating SWs but, more importantly, provides a definite assignment of SW mode number, thereby enabling a reliable determination of the spin stiffness constant with only two optically detected modes. The comprehensive model developed here, which comprises both Kerr and Voigt effects, provides useful guidelines (through Eq. 3) for optimizing the optical detection of SWs. It may also explain varying SW amplitude ratios observed in different layers/materials [2, 29]. It can be straightforwardly extended to longitudinal Kerr and Faraday effects, for which similar effect of the complex optical phase are expected, and therefore be applied to any kind of experimental geometry and magnetic layer, whether ferro-, ferri-, or antiferromagnetic, from metals to insulators.

We thank F. Perez and B. Jusserand for fruitful discussions, B. Eble for cryogenic data, B. Gallas for ellipsometric data, and M. Bernard, F. Margaillan, F. Breton, S. Majrab, C. Lelong for technical assistance. This work has been supported by UPMC (Emergence 2012), Region Ile-de-France (DIM Nano-K MURAS2012), and French ANR (ANR13-JS04-0001-01).

* e-mail: gourdon@insp.jussieu.fr

[1] E. Beaurepaire, J. Merle, a. Daunois, and J. Bigot, *Phys. Rev. Lett.* **76**, 4250 (1996).

[2] M. van Kampen, C. Jozsa, J. Kohlhepp, P. LeClair, L. Lagae, W. de Jonge, and B. Koopmans, *Phys. Rev. Lett.* **88**, 227201 (2002).

[3] J. Kisielewski, A. Kirilyuk, A. Stupakiewicz, A. Maziewski, A. Kimel, T. Rasing, L. T. Baczewski, and A. Wawro, *Phys. Rev. B* **85**, 184429 (2012).

[4] D. Wang, Y. Ren, X. Liu, J. Furdyna, M. Grimsditch, and R. Merlin, *Phys. Rev. B* **75**, 233308 (2007).

[5] Y. Hashimoto, S. Kobayashi, and H. Munekata, *Phys. Rev. Lett.* **100**, 067202 (2008).

[6] J. Qi, Y. Xu, a. Steigerwald, X. Liu, J. Furdyna, I. Perakis, and N. Tolk, *Phys. Rev. B* **79**, 085304 (2009).

[7] E. Rozkotova, P. Nemec, P. Horodyska, D. Sprinzl, F. Trojanek, P. Maly, V. Novak, K. Olejnik, M. Cukr, and T. Jungwirth, *Appl. Phys. Lett.* **92**, 122507 (2008).

[8] S. Shihab, H. Riahi, L. Thevenard, H. J. von Bardeleben, A. Lemaître, and C. Gourdon, *Appl. Phys. Lett.* **106**, 142408 (2015).

[9] P. Němec, V. Novák, N. Tesařová, E. Rozkotová, H. Reichlová, D. Butkovičová, F. Trojánek, K. Olejník, P. Malý, R. P. Campion, B. L. Gallagher, J. Sinova, and T. Jungwirth, *Nat. commun.* **4**, 1422 (2013).

[10] F. Hansteen, A. Kimel, A. Kirilyuk, and T. Rasing, *Phys. Rev. Lett.* **95**, 1 (2005).

[11] A. Kirilyuk, A. V. Kimel, and T. Rasing, *Rep. Prog. Phys.* **76**, 026501 (2013).

[12] S. Mangin, M. Gottwald, C.-H. Lambert, D. Steil, V. Uhlí, L. Pang, M. Hehn, S. Alebrand, M. Cinchetti, G. Malinowski, Y. Fainman, M. Aeschlimann, and E. E. Fullerton, *Nat. Mat.* **13**, 286 (2014).

[13] Y. Kajiwara, K. Harii, S. Takahashi, J. Ohe, K. Uchida, M. Mizuguchi, H. Umezawa, H. Kawai, K. Ando, K. Takanashi, S. Maekawa, and E. Saitoh, *Nature* **464**, 262 (2010).

[14] B. Lenk, H. Ulrichs, F. Garbs, and M. Mnzenberg, *Phys. Rep.* **507**, 107 (2011).

[15] S. O. Demokritov, B. Hillebrands, and A. N. Slavin, *Phys. Rep.* **348**, 441 (2001).

[16] E. Rozkotova, P. Nemec, N. Tesarova, P. Maly, V. Novak, K. Olejnik, M. Cukr, and T. Jungwirth, *Appl. Phys. Lett.* **93**, 232505 (2008).

[17] Y. Hashimoto and H. Munekata, *Appl. Phys. Lett.* **93**, 202506 (2008).

[18] F. Teppe, M. Vladimirova, D. Scalbert, M. Nawrocki, and J. Cibert, *Sol. St. Com.* **128**, 403 (2003).

[19] N. Tesařová, P. Nêmec, E. Rozkotová, J. Šubrt, H. Reichlová, D. Butkovičová, F. Trojánek, P. Malý, V. Novák, and T. Jungwirth, *Appl. Phys. Lett.* **100**, 102403 (2012).

[20] A. Kalashnikova, A. Kimel, R. Pisarev, V. Gridnev, P. Usachev, A. Kirilyuk, and T. Rasing, *Phys. Rev. B* **78**, 104301 (2008).

[21] Z. Liu, F. Giesen, X. Zhu, R. D. Sydora, and M. R. Freeman, *Phys. Rev. Lett.* **98**, 87201 (2007).

[22] M. Bombeck, A. S. Salasyuk, B. A. Glavin, A. V. Scherbakov, C. Brüggemann, D. R. Yakovlev,V. F. Sapega, X. Liu, J. K. Furdyna, A. V. Akimov,and M. Bayer, *Phys. Rev. B* **85**, 195324 (2012).

[23] J. Hamrle, J. Pištora, B. Hillebrands, B. Lenk, and M. Münzenberg, *J. Phys. D: Appl. Phys.* **43**, 325004 (2010).

[24] C. Kittel, *Phys. Rev.* **110**, 2139 (1958).

[25] J. Wu,N. D. Hughes,J. R. Moore,and R. J. Hicken *J. Magn. Magn. Mater.* **241**, 96 (2002).

[26] X. Liu and J. K. Furdyna, *J.Phys.: Cond. Mat.* **18**, R245 (2006).

[27] J. Zemen, J. Kučera, K. Olejník, and T. Jungwirth, *Phys. Rev. B* **80**, 1 (2009).

[28] M. Cubukcu, H. J. von Bardeleben, J. L. Cantin, and A. Lemaître, *Appl. Phys. Lett.* **96**, 102502 (2010).

[29] N. Tesařová, D. Butkovičová, R. P. Campion, A. W. Rushforth, K. W. Edmonds, P. Wadley, B. L. Gallagher, E. Schmoranzerová, F. Trojánek, P. Malý, P. Motloch, V. Novák, T. Jungwirth, and

P. Němec, *Phys. Rev. B* **90**, 155203 (2014).
[30] S. Shihab, L. Thevenard, A. Lemaître, J.-Y. Duquesne, and C. Gourdon, *J. Appl. Phys.* **119**, 153904 (2016).
[31] A. V. Kimel, G. V. Astakhov, a. Kirilyuk, G. M. Schott, G. Karczewski, W. Ossau, G. Schmidt, L. W. Molenkamp, and T. Rasing, *Phys. Rev. Lett.* **94**, 227203 (2005).
[32] N. Tesařová, P. Němec, E. Rozkotová, J. Zemen, T. Janda, D. Butkovičová, F. Trojánek, K. Olejník, V. Novák, P. Malý, and T. Jungwirth, *Nat. Phot.* **7**, 492 (2013).
[33] G. Traeger, L. Wenzel, and a. Hubert, *Phys. Stat. Sol. (a)* **131**, 201 (1992).
[34] A. Hubert and G. Traeger, *J. Mag. Magn. Mat.* **124**, 185 (1993).
[35] G. Pénissard, P. Meyer, J. Ferré, and D. Renard, *J. Mag. Magn. Mat.* **146**, 55 (1995).
[36] H. Terada, S. Ohya, and M. Tanaka, *Appl. Phys. Lett.* **106**, 222406 (2015).
[37] C. Gourdon, V. Jeudy, M. Menant, D. Roditchev, L. A. Tu, E. L. Ivchenko, and G. Karczewski, *Appl. Phys. Lett.* **82**, 230 (2003).
[38] M. Inoue, K. Arai, T. Fujii, and M. Abe, *J. Appl. Phys.* **83**, 6768 (1998).
[39] I. L. Lyubchanskii, N. N. Dadoenkova, M. I. Lyubchanskii, E. a. Shapovalov, and T. Rasing, *J. Phys. D: Appl. Phys.* **36**, R277 (2003).